RESEARCH ARTICLE

Wideband 1-Bit Bandpass Delta Sigma Modulator Using Elliptic Filter in Noise Transfer Function

TAKASHI MAEHATA [1,2], **(Member, IEEE), AND NORIHARU SUEMATSU**[2]**, (Senior Member, IEEE)**
[1]Transmission Devices Laboratory, Sumitomo Electric Industries Ltd., Yokohama 244-8588, Japan
[2]Research Institute of Electrical Communication, Tohoku University, Sendai 980-8577, Japan

Corresponding author: Takashi Maehata (maehata-takashi@sei.co.jp)

ABSTRACT A 1-bit band-pass delta-sigma modulator (BP-DSM), which utilizes oversampling technology, allows a modulated signal to be directly output by using a high-speed 1-bit digital pulse train, thus realizing miniaturization of transmitters. For 1-bit BP-DSM, the noise transfer function (NTF) is used to suppress quantization noise power in the transmission band and a guideline of out-of-band gain of |NTF| < 1.5 is used to prevent oscillation. However, in previous studies, such as Butterworth and inverse Chebyshev filters, the out-of-band gain was designed indirectly by tuning the zeros and poles in the transmission band and thus, was not stabilized sufficiently. Furthermore, even though the zeros of the NTF are identical to the poles of the loop filter, there are still widely used designs in which the zeros are set on the unit circle, making stabilization quite difficult. Therefore, in this paper, we propose a feasible implementation of the NTF for 1-bit BP-DSM with an elliptic filter that can be used to set not only in-band but also out-of-band gain, in which both the zeros and poles are set inside the unit circle. As a design result, a modulation bandwidth of 400 MHz as a relative bandwidth of 11%, a noise suppression bandwidth of 800 MHz, and an adjacent channel leakage power ratio of 50 dB were achieved at a center frequency of 3.6 GHz, enabling a wider bandwidth and higher SNR than before by improving the stability.

INDEX TERMS Delta-sigma modulator, quantization, 5G mobile communication, software defined radio, wideband.

I. INTRODUCTION

In 5G and next generation mobile communication systems, to achieve high-speed communication [1], [2], massive multiple-input and multiple-output (MIMO) and carrier aggregation (CA) [3] that use multiple transmitters have been introduced with a wideband modulation signal, which causes an increase in the size of equipment, thereby requiring a reduction in size. Moreover, this trend is predicted to keep going, and modulation signal bandwidth is expected to be more than several 100MHz, with an ever-increasing number of transmitters. To realize miniaturization of transmitters, it is important to suppress unexpected interference between multiple high-frequency analog circuits (analog mixer, local oscillator, etc.) in the equipment. This is a challenge to be met with miniaturization.

The associate editor coordinating the review of this manuscript and approving it for publication was Di Zhang.

However, since miniaturization is related to the scaling law for voltage, it is inevitable to take countermeasures for low voltage as well as for miniaturization. To cope with the low voltage issue, the signal-to-noise power ratio has to be maintained from the voltage direction to the time direction. 1-bit delta-sigma modulators, using an oversampling technique, which can convert wireless signals into a high-speed 1-bit digital pulse train, have been focused on. The 1-bit digital RF transmitter can output directly from the digital components as a high-speed 1-bit digital pulse train at several Gb/s and eliminates the need for analog radio-frequency components and their peripheral circuits, and thus avoids interference generated by them.

In delta-sigma modulator, using oversampling techniques to achieve high SNR, there are three types of methods: low-pass delta-sigma modulator (LP-DSM [4]–[11]), envelope-based delta-sigma modulator (E-DSM [12]–[14]), and band-pass delta-sigma modulator (BP-DSM [15]–[27]).
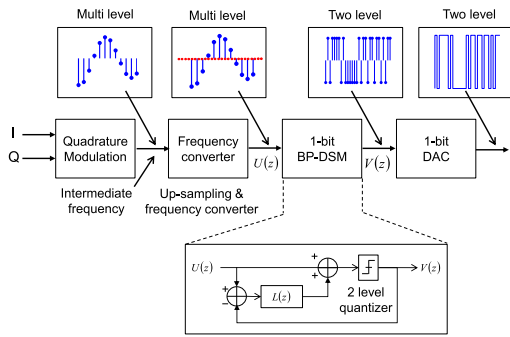
FIGURE 1. General block diagram of all-digital transmitters using a 1-bit bandpass delta sigma modulator.

E-DSM has reportedly been applied to MIMO radar using a direct digital synthesizer (DSS) or voltage-controlled oscillator (VCO) as the local oscillator. Both E-DSM and LP-DSM have a structure where digital data is generated by multiplying the local oscillator and the data rate is proportional to the carrier frequency, thus only single carrier transmission can be realized, not multi-carrier transmission. Naturally, changing the carrier frequency will not allow the same values for data rate, oversampling rate, or SNR.

On the other hand, BP-DSM as shown in Fig. 1, converts a quadrature modulated signal into a high-speed 1-bit digital train. The data rate of the train can be set independently of the carrier frequency, thereby achieving concurrent multicarrier transmissions [22]–[24] such as intercarrier aggregation, and is being considered for radio on fiber (RoF) [28] and next generation base stations [29]. The carrier frequency can be placed anywhere within the first Nyquist zone as defined by data rate, while keeping the same data rate and SNR.

Figure 2 shows trends in delta-sigma modulators over twenty years. Figure 2(a) shows the trend in modulation bandwidth, with widening starting in the 2000s and concurrent multi-band [22], realized in 2013. Figure 2(b) shows the trend in relative bandwidth, focusing on design where the adjacent channel leakage power ratio (ACLR) is more than 40 dB. The maximum relative bandwidth of the modulation signal is 5%. In 5G and next generation mobile communications, the modulation bandwidth will be wider and a larger relative bandwidth will be required. Following this trend, digital-to-analog converters (DACs) have become faster, and 6Gs/s DACs are now available in field programmable gate array (FPGA) devices. In addition, quadrature modulation is performed by utilizing the digital signal processing in FPGA, and the intermediate frequency or RF frequency is directly output at the DAC whose output frequency is below 3 GHz (first Nyquist zone). The 1-bit BP-DSM has also been demonstrated to output single-band and concurrent multi-band at RF frequencies including 3.5 GHz [23].

In the 1-bit BP-DSM, the noise transfer function (NTF) is designed to suppress in-band quantization noise to achieve
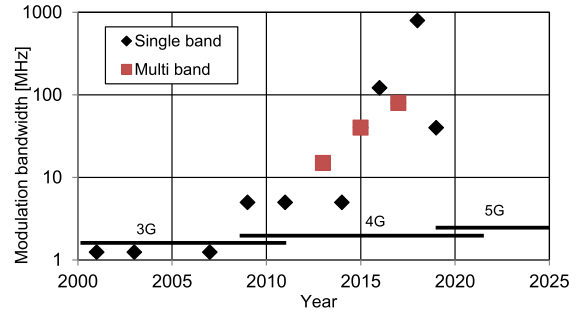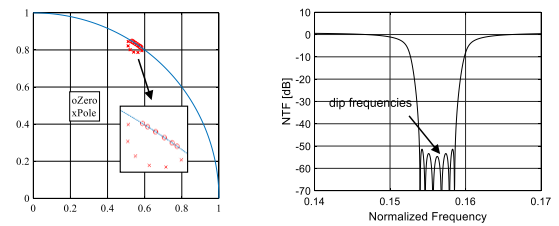

(a)   Modulation bandwidth trends over 20 years.
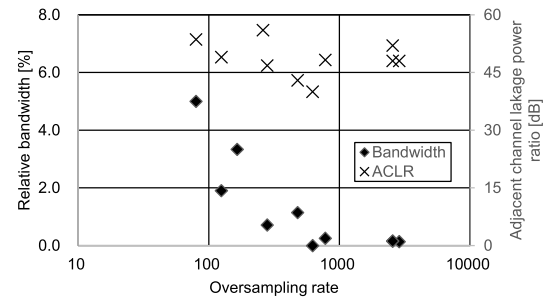
(b)   Relative bandwidth trends as a function of oversampling rate focusing on mobile communication where the adjacent channel leakage power ratio is more than 40 dB

FIGURE 2. Trends in delta modulation.

(a) Zero and pole map   (b) Frequency response of NTF

FIGURE 3. Typical frequency response example of the noise transfer function with a 6th-order filter using the poles and zeros of the left-hand side map.

wide bandwidth and high SNR. In the design of the noise transfer function, the guideline is that the out-of-band gain should be less than 1.5 to prevent oscillation [30], [31]. However, in the design of conventional NTFs, as shown in Fig. 3, a Butterworth filter or an inverse Chebyshev filter [4]–[27] is used, in which the zeros and poles are located only within the band, and the out-of-band gain is designed indirectly by adjusting them minutely. Consequently, when widening the bandwidth or increasing the SNR, design becomes difficult due to an increase of out-of-band gain.

To design zeros and poles in the NTF, a stability analysis of the modulator model as linear matrix inequalities (LMI) via the Kalman-Yakubovich-Popov (KPY) lemma was done as described in [31]–[34]. Unfortunately, these stabilization studies focus on unmodulated signals with no instantaneous power fluctuations, not modulated signals. For modulated LTE signals, a wider noise suppression bandwidth 3-5
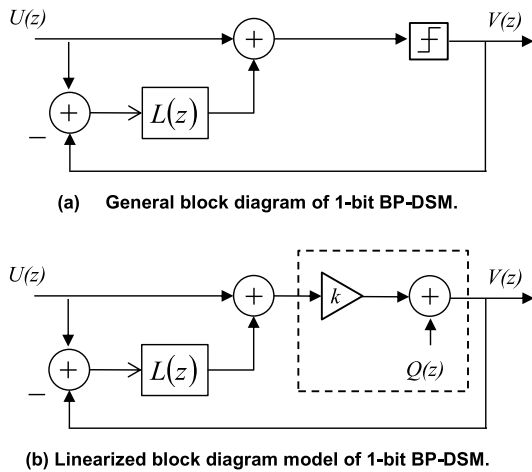
(a)   General block diagram of 1-bit BP-DSM.

(b) Linearized block diagram model of 1-bit BP-DSM.

FIGURE 4. Linearized block diagram of 1-bit BP-DSM as a linear model with quantization gain and additive quantization noise.

times wider is required, up to both sidebands and the next adjacent sidebands, of the modulated signal, and with large instantaneous power fluctuation.

In this paper, we propose a feasible implementation of the noise transfer function for 1-bit BP-DSM with an elliptic filter that can be used to set not only in-band but also out-of-band gain to transmit wideband LTE signals. The stability of the NTF was analyzed using a quantizer linearization model [35]–[37] as shown in Fig. 4. The quantizer linear model is based on the fact that the quantizer gain decreases inversely proportional to the quantizer input increasing because the quantizer output is still binary with constant amplitude. Based on a model in which loop gain in the feedback loop varies with input power, the locus of the poles for input power is estimated, and the stability is verified by checking that the locus of the poles is located within the unit circle.

II. BANDPASS DELTA SIGMA MODULATOR
Figure 1 shows a block diagram of a 1-bit BP-DSM. The in-phase and quadrature-phase baseband signals are quadrature modulated and output at intermediate frequency. The quadrature modulated signals are up-sampled and frequency converted through the digital frequency converter, and output as multi-level digitized RF signals. Conventionally, the up-sampling rate used is around 100 times the modulation bandwidth. In the frequency converter, the input signal is converted into pulses using an oversampling technique that inserts zeros, and frequency conversion is performed in the frequency domain using the generation of a large number of aliases, so that up-sampling and frequency conversion can be performed with almost no digital signal processing load, simultaneously. The carrier frequency can be defined by the aliased nth frequency, which is generated based on the intermediate frequency tunable by means of a quadrature modulator. The multi-level digitized RF signal is input to the 1-bit BP-DSM, converted to binary, and output. This binary

digital data is output as an analog waveform with a non-return-to-zero (NRZ) via a pulse generator (or 1-bit digital-to-analog converter). The waveform of the signal is regenerated through an analog band-pass filter and then transmitted from the antenna.

We now focus again on the block diagram of the 1-bit BP-DSM shown in Fig. 4(a). The input signal U(z) is output as the output signal V(z) through the binary quantizer, and the difference between the input and the output signals (quantization noise Q) makes feedback through the loop filter L(z). The output signal V(z) can be expressed by (1).

$$V(z) = U(z) + NTF(z) Q(z) \tag{1}$$

$$NTF(z) = \frac{1}{1 + L(z)} \tag{2}$$

The second term in (1), the quantization noise Q(z) has a noise transfer function (NTF) as an infinite response filter, having real number coefficients and is related to the loop filter L(z) as in (2). The NTF(z) is designed as a digital filter with a band rejection filter in the transmission band, and the second term in (1) suppresses the quantization noise in the signal band to achieve high SNR in the band. The band rejection filter can be designed as a single-band and/or multi-band filter to suppress the quantization noise to realize a concurrent multi-band modulator [22]–[24].

A. PLACEMENT OF ZEROS AND POLES
The 1-bit BP-DSM uses a noise transfer function to suppress the quantization noise in the signal band. In the design of the noise transfer function, the Lee criteria [30] guideline (|NTF| < 1.5) is used to ensure the stability of the feedback loop in the out-of-band gain. In this paper, to handle wider bandwidth signals, we propose a new method to handle the noise transfer function with both the in-band and the out-of-band gains by using an elliptic filter. The elliptic filters have a narrow transition region because the zeros are also placed in the rejection region.

Here, we again focus on the zeros of the noise transfer function of the conventional design. As shown in Fig. 3, the zeros are located on the unit circle [38], and an effect is observed where the power spectrum of the quantization noise is suppressed steeply in the band.

The noise transfer function as the numerator polynomial N(z), denominator polynomial D(z) is given in (3), the loop filter L(z) is expressed as (4), where the poles of the loop filter correspond to the zeros of the noise transfer function and are located on the unit circle. For stability, the poles have to be placed within the unit circle, and it is desirable to place them inside the unit circle rather than on the unit circle. Especially in BP-DSM, it is known that the poles move with input power [35], [37].

$$NTF(z) = \frac{N(z)}{D(z)} \tag{3}$$

$$L(z) = \frac{D(z) - N(z)}{N(z)} \tag{4}$$

Figure 4(b) shows a linearized block diagram of BP-DSM including a binary quantizer [26]. Here, the binary quantizer is represented as a linear model with quantization gain and additive quantization noise. From this model, the effective noise transfer function and the loop filter can be derived as (5) and (6). Here, the quantizer gain k can be derived as (7) where minimizing the mean square of the quantizer input and output errors, and E[x] denoting the mean value for x. The quantization gain k decreases with the increase of the input signal r because the output of the quantizer is binary (± 1) with constant amplitude, and this can be seen in (7). Moreover, it can be understood from (5) that the decrease in quantizer gain leads to the loss of quantization noise suppression performance.

$$NTF_k = \frac{1}{1 + kL} \qquad (5)$$

$$NTF_k = \frac{N(z)}{N(z) + k\{D(z) - N(z)\}} \qquad (6)$$

$$k = \frac{E[|r|]}{E[r^2]} \qquad (7)$$

Here, we focus on the input to the quantizer for achieving wide bandwidth and high SNR. To improve the suppression of quantization noise in the signal band, we should increase the gain of the loop filter L(z) in (2). This results in an increasing input to the quantizer, as seen in Fig. 4. However, since the output of the quantizer is constant amplitude, the quantizer gain k decreases as given in (7), and the effective loop filter gain kL, given in (5), is limited. If the loop gain is further increased, an overload occurs to the quantizer, the quantizer gain is reduced to almost zero, the effective loop gain kL is decreased, quantizer noise suppression performance is degraded by (5), and this causes further overload to the quantizer. This vicious cycle causes a large overload to the quantizer, leading to oscillation.

In other words, if 1-bit delta-sigma modulator is used within a range that does not overload the quantizer ($|r| < 1$), Equation (7) shows that the quantizer gain k has to be greater than or equal to 1 to ensure stability. Then, from (5), the effective loop gain kL approaches L approximately, and the achievable SNR upper bound is determined by the noise transfer function at the time of design.

To further understand the stability, we consider the root locus of the poles of the noise transfer function, shown in (6), based on the quantization gain k. Equation (6) becomes identical to (3) when k = 1. The root of the noise transfer function is the same as the poles in (3), and when k = 0, it moves to the zeros, mapped on the unit circle in (3), thus the root moves in the unit circle [35], depending on the magnitude of the input signal. To make the feedback system stable, the root locus has to be inside the unit circle, so it is more desirable to place the zeros inside the unit circle.

On the other hand, two issues arise if the zeros are placed inside the unit circle: the first issue is the disappearance of
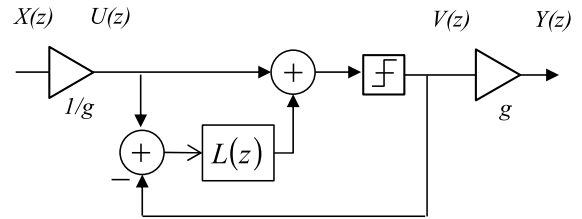

FIGURE 5. Proposed block diagram of 1-bit BP-DSM using an elliptic filter in NTF.
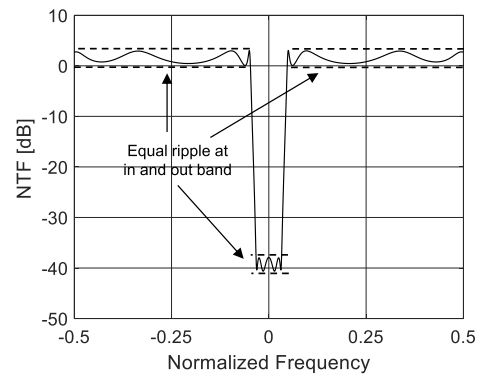

FIGURE 6. Frequency response of NTF with a 7th-order elliptic filter.

the sharp drop in the signal band, shown in Fig. 3. However, this does not cause a practical problem when considering a modulated signal with bandwidth, because quantization noise is integrated over the bandwidth and evaluated as adjacent channel leakage power.

The second issue is the feasibility of the loop filter. As shown in Fig. 4, the NTF is implemented by the loop filter, which is placed in the feedback loop and thus requires a delay of at least one clock. This causes significant difficulty in designing the noise transfer function [26] because the numerator polynomial D(z)–N(z) of the loop filter, given by (4), has to have no constant term as a constraint. Hence, a new design method is proposed in the next section, which ensures the feasibility of the loop filter while keeping the placement of the zeros inside the unit circle to improve stability.

B. NOISE TRANSFER FUNCTION

Equation (8) is used as the noise transfer function of the elliptic filter [39], [40], where p_n, q_n, $g > 0$ is real number and g is the collection of the constant terms in the numerator and denominator so that they equal 1. As mentioned in the section above, if g is not equal to 1, it's impossible to implement the loop filter by using the model in Fig.4 because the numerator polynomial of the loop filter, given by (4), has constant term. The loop filter is placed in the feedback loop and requires a delay of at least one clock.

In this paper, we manage to design an elliptic filter based on the noise transfer function, given in (8) and so propose a new feasible 1-bit BP-DSM block diagram, including the
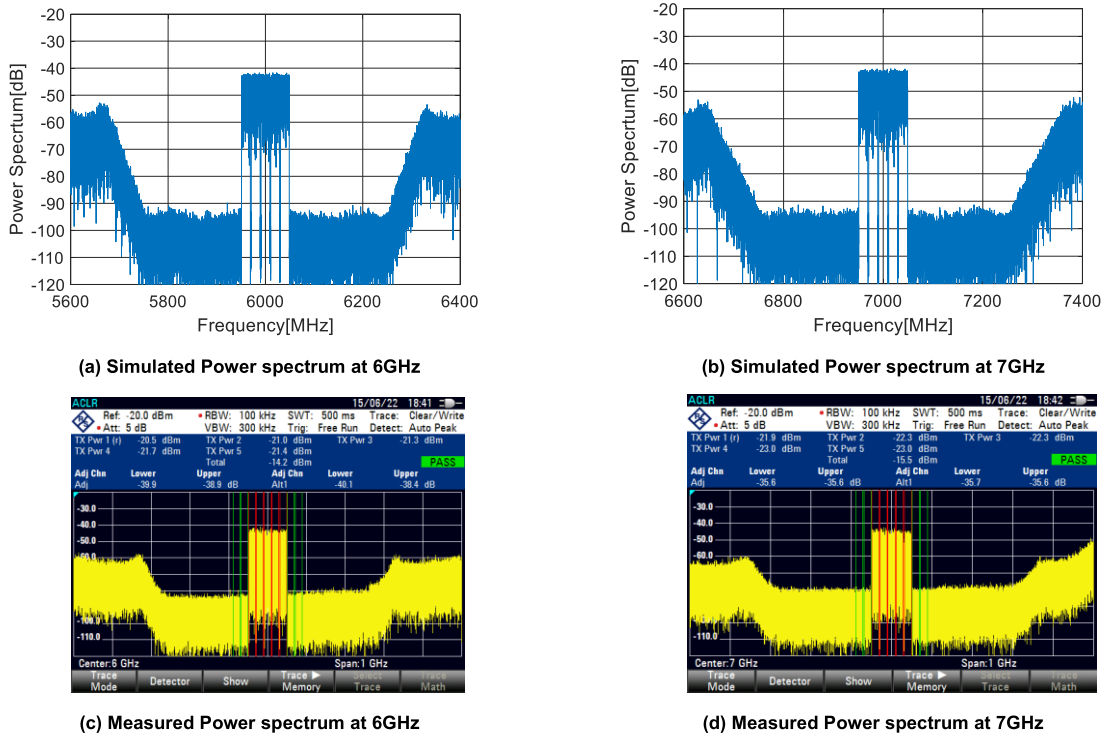
(a) Simulated Power spectrum at 6GHz

(b) Simulated Power spectrum at 7GHz

(c) Measured Power spectrum at 6GHz

(d) Measured Power spectrum at 7GHz

FIGURE 7. Simulated and measured adjacent channel leakage power ratio of a modulation bandwidth of 100 MHz based on 1-bit BP-DSM, using a 10th-order elliptic filter in noise transfer function and a data rate of 15 Gs/s.

elliptic filter in Fig. 5.

$$NTF_g = g \frac{1 + \sum_n q_n z^{-n}}{1 + \sum_n p_n z^{-n}} \tag{8}$$

$$NTF = \frac{1 + \sum_n q_n z^{-n}}{1 + \sum_n p_n z^{-n}} \tag{9}$$

$$V = U + NTFQ \tag{10}$$

$$L = \frac{\sum_{n=1} (p_n - q_n) z^{-n}}{1 + \sum_{n=1} q_n z^{-n}} \tag{11}$$

$$|U| <= 1, \quad V = \pm 1 \tag{12}$$

$$Y = X + gNTF \quad Q = X + NTF_g Q \tag{13}$$

Figure 5 shows that the quantization noise generated by the binary quantizer is Q. The input U and output V are given by (9) and (10), respectively, and the loop filter is given by (11) by substituting (9) into (2), and the input and output signals U and V are used within the range of (12). The input X and output Y can be expressed as (13), where g is corresponding to the scaling factor for the input and output signals X and Y in Fig.5. Since the stability of the feedback loop is determined by the poles of the noise transfer function NTF, we also use Lee's criterion guideline ($|NTF| < 1.5$) in this paper to ensure stability.

Next, we consider the loop filter L(z) given by (11). The loop filter does not include a constant term, indicating that a single delay is inserted between its inputs and outputs. The single delay makes it possible to implement the filter as a digital filter in a feedback loop that includes the loop filter, thus realizing a 1-bit BP-DSM using an elliptic filter as shown in the block diagram in Fig. 5.

The conventional noise transfer functions have been reported to concentrate zeros at DC location on the unit circle or to optimally place them on the unit circle to minimize the quantization noise in the signal band [35]. All of these design cases [4]–[27] can be expressed as the noise transfer function with g set to 1 in (8). This means that Eq. (8) and Fig. 5 include a subset of conventional delta-sigma modulators where the scaling g is set to 1, and Figure 5 is an extension of the conventional delta-sigma modulator.

C. NTF DESIGN PROCEDURE
In this section, the procedure for designing a noise transfer function using an elliptic filter is presented.

1. Specify the filter order and oversampling rate, and calculate the filter response at the normalized frequency.

2. Design a high-pass elliptic filter [36], [37] using Lee's guideline, specifying the quantization noise suppression bandwidth, suppression level, and ripple inside and outside the bandwidth. In the appendix, NTF design in the frequency domain is shown numerically and efficiently by using a numerical solver like MATLAB.

3. Summarize the designed noise transfer function in the form of (8) so that the constant terms in the numerator and denominator are 1.

4. Transform the noise transfer function to a band suppression filter using a high-pass elliptic filter as a prototype filter [26].

$$
\begin{cases}
z \rightarrow -z\dfrac{z+\alpha}{\alpha z+1}, \quad \alpha = \text{-cos}\left(2\pi\dfrac{f_0}{f_s}\right) \\
NTF\,(z) \rightarrow NTF\left(-z\dfrac{z+\alpha}{\alpha z+1}\right) = NTF\,(z,\alpha)
\end{cases}
\tag{14}
$$

5. Based on the loop filter L(z) calculated by (11) and the block diagram in Fig. 5, sweep the input amplitude and check the maximum achievable SNR by simulation. Also, confirm that the quantization gain k is greater than or equal to 1 using (7).

6. Gradually increase the quantization noise suppression bandwidth and suppression level, and repeat steps 2-5 to maximize the achievable SNR.

7. If the target SNR is not reached, increase the filter order and oversampling rate, and repeat steps 1-7.

The NTF design procedure, described above, enables us to detail the parameters of the modulator to get the achievable SNR. Unfortunately, 1-bit BP-DSM is a nonlinear process that includes a 1-bit quantizer in the feedback loop, and thus should be fully verified through many simulations.

III. DESIGN RESULT

This section shows some examples of elliptic filters that were designed following the procedure described in the previous section. Figure 6 shows the design of a 7th-order elliptic filter, which has equal ripple characteristics in and out of the band and steep filter characteristics. This indicates that the zeros are located inside the unit circle as there is a disappearance of the sharp drop in the signal band.

This desired effect is produced by designing equal ripple characteristics in the band in design procedure 2. Next, using the transformation for frequency in design procedure 4, figures 7(a) and (b) show the simulated power spectra which are based on 1-bit BP-DSM with a 10th-order elliptic filter at a data rate of 15 Gb/s, modulation bandwidth of 100 MHz (5 LTE signals with the same bandwidth), a noise suppression bandwidth of 500 MHz, and center frequencies of 6 GHz and 7 GHz, respectively. A 1-bit digital data train was generated, based on Fig. 5.

Figures 7(a) and 7(b) show that the ACLR and the next ACLR are both about 50 dB, and the two power spectra have almost the same shape. This is because of the effect of performing the transformation in design procedure 4, which shows that the power spectra have almost the same shape at other frequencies as well. This transformation preserves the amplitude ripple and phase characteristics of the filter. For a mobile phone communication system, there are many frequency bands and the performance has to be the same in
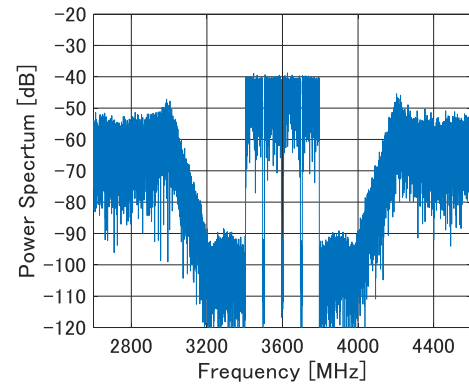
(a) Simulated Power spectrum at 3.6 GHz with a 6th-order elliptic filter and 70 times oversampling.
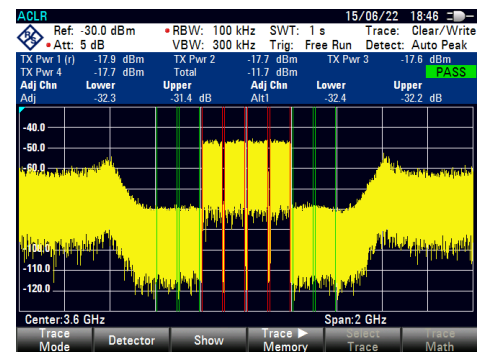
(b) Measured Power spectrum at 3.6 GHz with a 6th-order elliptic filter and 70 times oversampling.
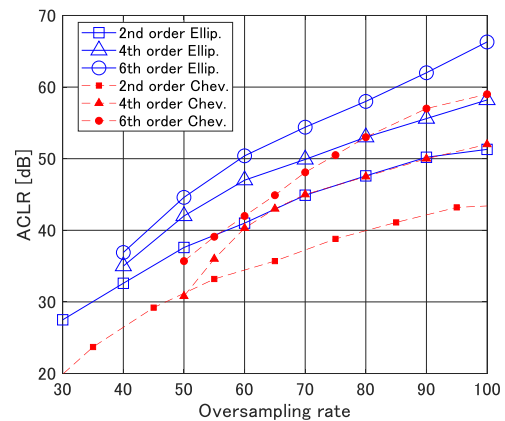
(c) Simulated ACLR using sevral oversampling rate and filter orders.

FIGURE 8. Simulated and measured adjacent channel leakage power ratio of a modulation bandwidth of 400 MHz (4 LTE signals with the same bandwidth) and a noise suppression bandwidth of 800 MHz at a center frequency of 1/4 of the oversampling rate.

all frequency bands, so the transformation method is suitable for this application.

In figures 7(c) and 7(d), the power spectra are measured to correspond to Figures 7(a) and 7(b), respectively, which are generated by a Keysight M9502A pulse pattern generator at a data rate of 15 Gb/s, after downloading the binary data, based on Fig.5. The ACLR in Figures 7(c) and 7(d) are 39 dB, 36 dB, respectively.

TABLE 1. State-of-the-art of delta-sigma modulator.

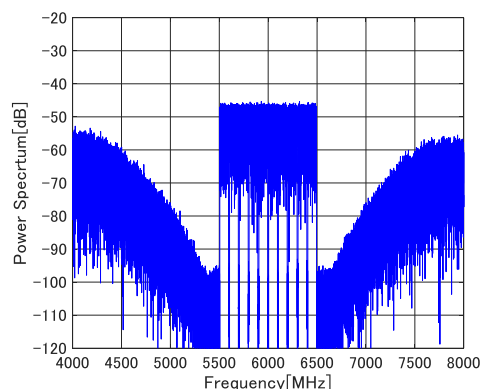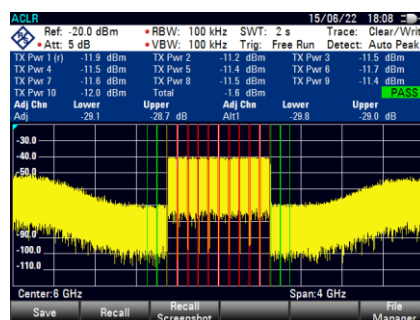| Reference	BW [MHz]	fs [GHz]	OSR	Fc [GHz]	BW/Fc [%]	ACLR [dB]	Implementation	Type	Signal type
[7]	5	4	80	1.0	5.0	53.6	CMOS 90nm	LP	UMTS
[11]	40	19.2	480	3.5	1.1	43	FPGA	LP	local-5G
[13]	5	1.4	780	2.0	0.3	48.3	CMOS 90nm	EP	LTE
[14]	5	3.6	280	0.7	0.7	46.8	CMOS 90nm	EP	LTE
[18]	1.25	1	2880	0.9	0.1	48	AWG(PCI-344)	BP	IS-95 CDMA
[19]	1.25	3.2	2560	0.8	0.2	48	CMOS(Domino Logic)	BP	IS-95 CDMA
[21]	1.25	3.2	2560	0.8	0.2	52	PPG(Agilent 81134A)	BP	IS-95 CDMA
[22]	5/5/5	3.9	260	0.8/1.5/1.8		56 45	Simulation FPGA:Stratix IV	BP+BP+BP	LTE
[23]	20/20	25	625	0.8/1.4		40	AWG	BP+BP	LTE
[24]	80	10	125	2.1/3.5		49	AWG(Tektronix:AWG7102)	BP+BP	LTE
[41]	100	16.5	165	3.0	3.3	30	CMOS 90nm	EP	LTE(100MHzx1)
This work	400	25.6	70	3.6	11.1	50.3 31.4	Simulation Keysight:M9502A	BP	LTE(100MHzx4)
This work	1000	64	64	6.0	16.7	50.5 28.7	Simulation Keysight:M9502A	BP	LTE(100MHzx10)
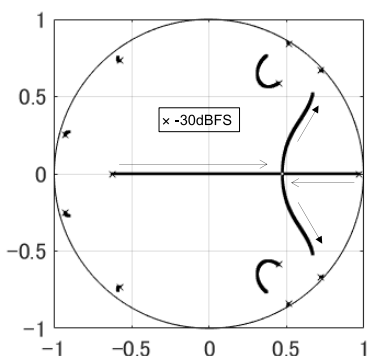
FIGURE 9. Root locus of a six-order modulator according to the input power from −30dBFS to 0 dBFS. The simulations used a modulation bandwidth of 400 MHz (4 LTE signals with the same bandwidth) and a noise suppression bandwidth of 800 MHz.

(a)   Simulated Power spectrum at 6 GHz

(b)   Measured Power spectrum at 6 GHz

FIGURE 10. Simulated and measured adjacent channel leakage power ratio of a modulation bandwidth of 1000 MHz (10 LTE signals with the same bandwidth) and a noise suppression bandwidth of 1400 MHz, a 6th-order elliptic filter, and 64 times oversampling.

Figures 8(a) and (b) show the simulated and measured power spectra, using a modulation bandwidth of 400 MHz (4 LTE signals with the same bandwidth), a noise suppression bandwidth of 800 MHz (including next adjacent channel bandwidth on both sides), and a center frequency of 3.6 GHz. Figures 8(a) and (b) show an example of a sixth-order elliptic filter with oversampling of 70. Figure 8(c) shows a maximum ACLR achieved by optimizing the oversampling rate and the order of the elliptic and Chebyshev filter at a center frequency of 1/4 of the oversampling rate.

Figures 8(a) and 8(b) show that the simulated and measured ACLR of 50 dB and 31dB are achieved, respectively, for a relative bandwidth of 11% (the ratio of the modulation bandwidth to the center frequency) and an oversampling rate of 70 times, including the adjacent channel. As shown

in Fig. 2(b) and Table 1, the proposed design exceeds the maximum relative bandwidth of 5% in the previous design

and also achieves a high SNR, indicating that the proposed elliptic filter can handle modulated signals with a larger relative bandwidth.

Figure 8(c) shows that the simulated ACLR increases in proportion to both the number of oversamples and the order of the filter. As can be seen ACLR, achieved by Chebyshev filters [26] or the proposed elliptic filter, the performance of the proposed elliptic filter is about 5 dB to 10 dB better than one of Chebyshev filter type. It is shown that to achieve an ACLR of 50 dB, a minimum of 60 times the number of oversamples is required for a sixth-order elliptic filter, while 75 times higher is required for a sixth-order Chebyshev filter.

Figure 9 shows the root locus of the noise transfer function as the input power is varied in Fig. 8(a). The root locus is shown in a range of 30 dB with the maximum input amplitude of 1 being 0 dBFS, corresponding to Fig. 5 and (6), and it is clear that the root locus is located inside the unit circle at all input powers and is thus stable.

Figures 10(a) and (b) show the simulated and measured ACLR of 50 dB and 28.7 dB, respectively, achieved with a modulation bandwidth of 1000 MHz (10 LTE signals with the same bandwidth), a noise suppression bandwidth of 1400 MHz, and a center frequency of 6GHz, with 64 times oversampling and a 6th-order filter.

This design example shows the result of optimization design based on Fig. 8(c) by 2.5 times modulation bandwidth, following design procedure. This design example confirms that the modulation bandwidth can be scaled based on the oversampling rate in Fig. 8(c). This means that 1-bit BP-DSM with an elliptic filter can be used to handle wider bandwidth modulation signals that will be required in the next generation of wireless communications.

IV. CONCLUSION

In 5G and next generation mobile communication systems, a 1-bit band-pass delta-sigma modulator with an elliptic filter has been proposed for wideband modulation and high SNR. This work demonstrated that 1-bit BP-DSM with a 6th-order elliptic filter is able to achieve a center frequency of 3.6 GHz, modulation bandwidth of 400 MHz, a relative bandwidth of 11%, an oversampling rate of 70, and the simulated and measured ACLR of 50 dB and 31 dB, respectively. In the 1 GHz modulation bandwidth for the next generation mobile communication standard, it is also shown that the simulated and measured ACLR of 50 dB and 28.7 dB, respectively, can be achieved by using the same 64 times oversampling and 6th order elliptic filters.

APPENDIX NTF DESIGN IN FREQUENCY DOMAIN

The design flow of a NTF for a 1-bit BP-DSM was done as follows. To avoid out-of-band oscillation, it is necessary to control the gain frequency response of the out-of-band NTF. This means that the magnitude of the NTF must be designed over the whole frequency range [−1/2fd, 1/2fd], where fd is the output data rate. For this reason, unlike an inverse

Chebyshev band stop filter, a NTF requires a kind of elliptical filter with equiripple behavior in both passband and stopband.

In this section, we introduce the design flow to control the magnitude frequency response of the NTF with the infinite response (IIR) filter. The design flow is based on linear programming design [36].

Equation (A-1) is a general type of NTF with IIR filter [26].

$$NTF(z) = \frac{N(z)}{D(z)} = \frac{\sum_{m=0}^{n} b_m z^{-m}}{\sum_{m=0}^{n} a_m z^{-m}} \quad \text{(A-1)}$$

Here, the numerator polynomial N(z) and the denominator polynomial D(z) are nth-degree polynomials.

$$|NTF(z)| \leq 1.5 \quad \text{(A-2)}$$

Equation (A-2) is Lee's criteria [30], which is used as a guideline for ensuring the stability of the delta sigma modulator in the frequency domain. In order to design the filter coefficients in (A-1) under the constraint in (A-2), the magnitude squared response of NTF(z) is obtained by substituting z = exp(jw) into (A-1), where w is normalized by the output data frequency fd.

$$|NTF(z)NTF(z^{-1})| = \frac{N(z)N(z^{-1})}{D(z)D(z^{-1})} \leq 1.5^2 \quad \text{(A-3)}$$

$$= \frac{\left(\sum_{m=0}^{n} b_m z^{-m}\right)\left(\sum_{m=0}^{n} b_m z^{m}\right)}{\left(\sum_{m=0}^{n} a_m z^{-m}\right)\left(\sum_{m=0}^{n} a_m z^{m}\right)} \quad \text{(A-4)}$$

$$= \frac{\sum_{m=-n}^{n} d_m z^{-m}}{\sum_{m=-n}^{n} c_m z^{-m}} \leq 1.5^2 \quad \text{(A-5)}$$

where

$$c_m = c_{-m} \quad \text{(A-6)}$$

$$d_m = d_{-m} \quad \text{(A-7)}$$

$$|NTF(z)NTF(z^{-1})| = |NTF(e^{jwt})NTF(e^{-jwt})| \quad \text{(A-8)}$$

$$\frac{d_0 + \sum_{m=1}^{n} 2d_m \cos(mw)}{c_0 + \sum_{m=1}^{n} 2c_m \cos(mw)} = \frac{\hat{N}(w)}{\hat{D}(w)} \leq 1.5^2 \quad \text{(A-9)}$$

where

$$\hat{N}(w) = d_0 + \sum_{m=0}^{n} 2d_m \cos(mw) \geq 0 \quad \text{(A-10)}$$

$$\hat{D}(w) = c_0 + \sum_{m=1}^{n} 2c_m \cos(mw) \geq 0 \quad \text{(A-11)}$$

As can be seen from (A-3) to (A-11), the stability condition in (A-2) limits the maximum of the squared absolute value of
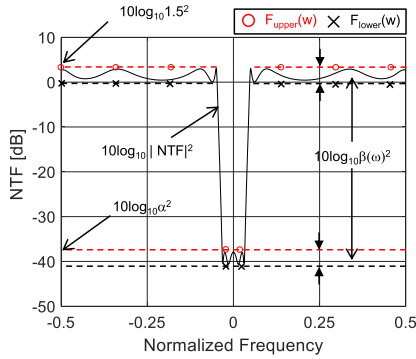
FIGURE 11. Specifications of NTF for designing an equiripple elliptical filter.

the NTF in (A-9) and it can also give a specification for the upper gain frequency response to design the filter in (A-12) and (A-13).

$$F_{upper}(w)\,\hat{D}(w) \geq \hat{N}(w) \geq 0 \tag{A-12}$$

$$F_{upper}(w) = \begin{cases} 1.5^2 & outside\ band \\ \alpha^2 & inside\ frequency\ band \end{cases} \tag{A-13}$$

Here, α^2 is a given minimum suppression level in the target frequency band, as shown in Fig.9.

Similarly, the lower gain frequency response of |NTF| 2 can be given by

$$\hat{N}(w) \geq F_{lower}(w)\,\hat{D}(w) \geq 0 \tag{A-14}$$

$$F_{lower}(w) = F_{upper}(w)\,\beta(w)^2 \tag{A-15}$$

where β^2 is the tolerance of the gain frequency response.

Thus, the linear inequalities in (A-10)–(A-15) are expressed as constraints to correspond to the filter specifications, as shown in Fig.11. They can be solved by using linear programming techniques such as the simplex or revised simplex algorithm. The resulting filter is a kind of an elliptic filter with equiripple behavior in both the passband and the stopband. After designing the above NTF, the loop filter L(z) is calculated by (11).

REFERENCES

[1] *Study on New Radio Access Technology: Radio Access Architecture and Interfaces*, document TR 38.801, V14.0.0, 3GPP, 2017.

[2] *NG-RAN: Architecture description*, document TS 38.401, 3GPP, 2018.

[3] *Evolved Universal Terrestrial Radio Access (E-UTRA); Physical Channels and Modulation*, document TS36.211, 3GPP, 2015. [Online]. Available: http://www.3gpp.org

[4] R. W. Adams, P. F. Ferguson, A. Ganesan, S. Vincelette, A. Volpe, and R. Libert, "Theory and practical implementation of a fifth-order sigma-delta A/D converter," *J. Audio Eng. Soc.*, vol. 39, nos. 7–8, pp. 515–528, 1991.

[5] S. Luschas, R. Schreier, and H.-S. Lee, "A 942 MHz output, 17.5 MHz bandwidth, −70 dBc IMD3 ΣΔ DAC," in *Proc. IEEE Custom Integr. Circuits Conf.*, Sep. 2003, pp. 21–24.

[6] R. F. Cordeiro, A. S. R. Oliveira, J. Vieira, and T. O. e Silva, "Wideband all-digital transmitter based on multicore DSM," in *IEEE MTT-S Int. Microw. Symp. Dig.*, May 2016, pp. 1–4.

[7] A. Frappe, A. Flament, B. Stefanelli, A. Kaiser, and A. Cathelin, "An all-digital RF signal generator using high-speed ΔΣ modulators," *IEEE J. Solid-State Circuits*, vol. 44, no. 10, pp. 2722–2732, Jan. 2009.

[8] A. Jerng and C. G. Sodini, "A wideband ΔΣ digital-RF modulator for high data rate transmitters," *IEEE J. Solid-State Circuits*, vol. 42, no. 8, pp. 1710–1722, Aug. 2007.

[9] D. C. Dinis, R. F. Cordeiro, A. S. R. Oliveira, J. Vieira, and T. O. Silva, "Improving the performance of all-digital transmitter based on parallel delta-sigma modulators through propagation of state registers," in *Proc. IEEE 60th Int. Midwest Symp. Circuits Syst. (MWSCAS)*, Aug. 2017, pp. 1133–1137.

[10] M. Tanio, S. Hori, N. Tawa, T. Kuwabara, and K. Kunihiro, "An FPGA-based 1-bit digital transmitter with 800-MHz bandwidth for 5G millimeter-wave active antenna systems," in *IEEE MTT-S Int. Microw. Symp. Dig.*, Jun. 2018, pp. 499–502.

[11] S. Hori, K. Motoi, T. Soma, H. Noguchi, S. Deb, M. Tanio, N. Tawa, T. Kaneko, and K. Kunihiro, "A 1-bit digital transmitter system using a 20-Gbps quadruple-cascode class-D digital power amplifier with 45 nm SOI CMOS," in *IEEE MTT-S Int. Microw. Symp. Dig.*, Jun. 2019, pp. 734–737.

[12] M. Tanio, S. Hori, N. Tawa, T. Yamase, and K. Kunihiro, "An FPGA based all-digital transmitter with 28-GHz time-interleaved delta-sigma modulation," in *IEEE MTT-S Int. Microw. Symp. Dig.*, May 2016, pp. 1–4.

[13] S. Hori, K. Kunihiro, K. Takahashi, and M. Fukaishi, "A 0.7–3 GHz envelope modulator using phase modulated carrier clock for multi-mode/band switching amplifiers," in *Proc. IEEE Radio Freq. Integr. Circuits Symp.*, Jun. 2011, pp. 1–4.

[14] M. Tanio, S. Hori, M. Hayakawa, N. Tawa, K. Motoi, and K. Kunihiro, "A linear and efficient 1-bit digital transmitter with envelope delta-sigma modulation for 700 MHz LTE," in *IEEE MTT-S Int. Microw. Symp. Dig.*, Jun. 2014.

[15] S. A. Jantzi, R. Schreier, and M. Snelgrove, "A bandpass ΣΔ A/D converter for a digital AM receiver," in *Proc. IEE Int. Conf. Analogue-to-Digital Digital-to-Analogue Conversion*, Swansea, U.K., Sep. 1991, pp. 75–80.

[16] S. A. Jantzi, M. Snelgrove, and P. F. Ferguson, "A 4th-order bandpass sigma-delta modulator," in *Proc. IEEE Custom Integr. Circuits Conf.*, May 1992, p. 16.

[17] L. Longo and B.-R. Horng, "A 15b 30 kHz bandpass sigma-delta modulator," in *IEEE Int. Solid-State Circuits Conf. (ISSCC) Dig. Tech. Papers*, Feb. 1993, pp. 226–227.

[18] M. P. Asbeck, E. L. Larson, and G. I. Galton, "Synergistic design of DSP and power amplifers for wireless communications," *IEEE Trans. Microw. Theory Techn.*, vol. 49, no. 11, pp. 2163–2169, Nov. 2001.

[19] J. Rode, J. Hinrichs, and P. Asbeck, "Transmitter architecture using digital generation of RF signals," in *Proc. Radio Wireless Conf. (RAWCON)*, Aug. 2003, pp. 245–248.

[20] J. Ketola, J. Sommarek, J. Vankka, and K. Halonen, "Transmitter utilising bandpass delta-sigma modulator and switching mode power amplifier," in *Proc. IEEE Int. Symp. Circuits Syst.*, May 200, pp. 633–636.

[21] T. P. Hung, J. Rode, L. E. Larson, and P. M. Asbeck, "Design of H-bridge class-D power amplifiers for digital pulse modulation transmitters," *IEEE Trans. Microw. Theory Techn.*, vol. 55, no. 12, pp. 2845–2855, Dec. 2007.

[22] T. Maehata, K. Totani, S. Kameda, and N. Suematsu, "Concurrent dualband 1-bit digital transmitter using band-pass delta-sigma modulator," in *Proc. Eur. Microw. Conf.*, 2013, pp. 1523–1526.

[23] S. Chung, R. Ma, S. Shinjo, and K. H. Teo, "Inter-band carrier aggregation digital transmitter architecture with concurrent multi-band delta-sigma modulation using out-of-band noise cancellation," in *IEEE MTT-S Int. Microw. Symp. Dig.*, May p2015, p. 1–4.

[24] T. Maehata, S. Kameda, and N. Suematsu, "1-bit band-pass delta-sigma modulator with parallel IIR form for concurrent multiband digital transmitter," *IEICE Trans. Commun.*, vol. 100, no. 7, pp. 1152–1159, 2017.

[25] R. Schreier and M. Snelgrove, "Bandpass delta-sigma modulation," *Electron. Lett.*, vol. 25, no. 23, pp. 1560–1561, Nov. 1989.

[26] R. Schreier and G. C. Temes, *Understanding Delta-Sigma Data Converters, Institute of Electrical and Electronics Engineers*. Hoboken, NJ, USA: Wiley, 2005.

[27] W. Kim, J. Rode, A. Scuderi, C. Park, P. M. Asbeck, and H. Son, "An efficient voltage-mode class-D power amplifier for digital transmitters with delta-sigma modulation," in *IEEE MTT-S Int. Microw. Symp. Dig.*, Jun. 2011, pp. 1–4.

[28] T. Maehata, S. Kameda, and N. Suematsu, "A novel channel coding scheme for digital RF transmitter comprising a 1-bit band-pass delta-sigma modulator," in *Proc. Asia–Pacific Microw. Conf. (APMC)*, Nov. 2014, pp. 932–934.

[29] J. Wang, Z. Jia, L. A. Campos, and C. Knittle, "Delta-sigma modulation for next generation fronthaul interface," *J. Lightw. Technol.*, vol. 37, no. 12, pp. 2838–2849, Jun. 2019.

[30] K. C.-H. Chao, S. Nadeem, W. L. Lee, and C. G. Sodini, "A higher order topology for interpolative modulators for oversampling A/D converters," *IEEE Trans. Circuits Syst.*, vol. 37, no. 3, pp. 309–318, Mar. 1990.

[31] M. Nagahara and Y. Yamamoto, "Frequency domain min-max optimization of noise-shaping delta-sigma modulators," *IEEE Trans. Signal Process.*, vol. 60, no. 6, pp. 2828–2839, Jun. 2012.

[32] X. Li, H. Gao, and C. Yu, "An iterative LMI approach to IIR noise transfer function optimization for delta-sigma modulators," in *Proc. Austral. Control Conf.*, Perth, WA, Australia, Nov. 2013, pp. 67–72.

[33] M. Sienko, "Loop-filter design and analysis for delta-sigma modulators and oversampled IIR filters," *IEEE Trans. Circuits Syst. I, Reg. Papers*, vol. 65, no. 12, pp. 4121–4132, Jun. 2018.

[34] S. Ohno, T. Shiraki, M. R. Tariq, and M. Nagahara, "Mean squared error analysis of quantizers with error feedback," *IEEE Trans. Signal Process.*, vol. 65, no. 22, pp. 5970–5981, Nov. 2017.

[35] S. Ardalan and J. Paulos, "An analysis of nonlinear behavior in delta–sigma modulators," *IEEE Trans. Circuits Syst.*, vol. CS-34, no. 6, pp. 593–603, Jun. 1987.

[36] G. I. Bourdopoulos, A. G. Pnevmatikakis, and T. L. Deliyannis, "Numerical method for determining the quantization error PDF of single-bit $\Sigma\Delta$ Modulators," *IEEE Trans. Circuits Syst. I, Reg. Papers*, vol. 51, no. 4, pp. 718–731, Apr. 2004.

[37] T. Ritoniemi, T. Karema, and H. Tenhunen, "The design of stable high order 1-bit sigma-delta modulators," in *Proc. IEEE Int.Symp. Circuits Sys.*, vol. 4, May 1990, pp. 3267–3270.

[38] R. Schreier, "An empirical study of high-order single-bit delta-sigma modulators," *IEEE Trans. Circuits Syst. II, Analog Digit. Signal Process.*, vol. 40, no. 8, pp. 461–466, Aug. 1993.

[39] L. Rabiner, N. Graham, and H. Helms, "Linear programming design of IIR digital filters with arbitrary magnitude function," *IEEE Trans. Acoust., Speech, Signal Process.*, vol. ASSP-22, no. 2, pp. 117–123, Apr. 1974.

[40] A. Gray and J. Markel, "A computer program for designing digital elliptic filters," *IEEE Trans. Acoust., Speech, Signal Process.*, vol. ASSP-24, no. 6, pp. 529–538, Dec. 1976.

[41] S. Hori, Y. Kase, N. Oshima, and K. Kunihiro, "Radio-over-fiber systems with 1-bit digital modulation for 5G/6G indoor wireless communication," in *Proc. Asia Pacific Wireless Commun. Symp. (APWCS)*, Aug. 2021, pp. 1–5.

TAKASHI MAEHATA (Member, IEEE) received the B.S. degree in electronic engineering from Kansai University, in 1992, the M.S. degree in electromagnetic energy engineering from Osaka University, in 1994, and the Ph.D. degree in electrical communication from Tohoku University, in 2018. He has been engaged in the research and development of OFDM implementations, LDPC codec, crest factor reduction, and digital pre-distortion for wireless communication and intelligent transport systems. He is currently a member of the Transmission Device Laboratory, Sumitomo Electric Industries Ltd., and also a Visiting Associate Professor of the Research Institute of Electrical Communication, Tohoku University.

NORIHARU SUEMATSU (Senior Member, IEEE) was born in Tokyo, Japan, in 1962. He received the B.S., M.S., and Dr.Eng. degrees in electronics and communication engineering from Waseda University, Tokyo, in 1985, 1987, and 2000, respectively. In 1987, he joined Mitsubishi Electric Corporation, Tokyo, where he was engaged in research and development on microwave and millimeter-wave solid-state circuits, including Si-MMICs/RFICs, linearizers, transceivers for cellular phones, ITS, and satellite communication systems. From 1992 to 1993, he was a Visiting Researcher with the University of Leeds, Leeds, U.K. Since 2010, he has been a Professor with the Research Institute of Electrical Communication, Tohoku University, Sendai, Japan. His current research interests include next generation wireless systems and hardware for terrestrial and satellite communications. He was a recipient of the Shinohara Award from the Institute of Electronics, Information and Communication Engineers (IEICE), in 1992, the Ohm Award from the Promotion Foundation for Electrical Science and Engineering, in 2002, the Prize for Science and Technology (Development Category) of the Commendation for Science and Technology by the Minister of Education, Culture, Sports, Science and Technology, Japan, in 2009, and the IEICE Electronic Society Award, in 2012. He is a fellow of the IEICE.

• • •